



Published in final edited form as:

*Nature*. 2010 December 9; 468(7325): 819–823. doi:10.1038/nature09551.

## Interdependence of behavioural variability and response to small stimuli in bacteria

Heungwon Park<sup>1</sup>, William Pontius<sup>2</sup>, Calin C. Guet<sup>3</sup>, John F. Marko<sup>4</sup>, Thierry Emonet<sup>2</sup>, and Philippe Cluzel<sup>3</sup>

<sup>1</sup>The James Franck Institute, The Institute for Biophysical Dynamics, and The Department of Physics, University of Chicago, Chicago, IL 60637, USA.

<sup>2</sup>Departments of Molecular, Cellular, and Developmental Biology & Physics, Yale University, New Haven, CT 06520, USA.

<sup>3</sup>FAS Center for Systems Biology and Department of Molecular and Cellular Biology, Harvard University, 52 Oxford St, Cambridge, MA 02138, USA.

<sup>4</sup>Department of Biochemistry, Molecular Biology, and Cell Biology and Department of Physics and Astronomy, Northwestern University, Evanston, IL 60208, USA.

### Abstract

The chemotaxis signalling network in *E. coli* that controls the locomotion of bacteria is a classic model system for signal transduction<sup>1–2</sup>. This pathway modulates the behaviour of flagellar motors to propel bacteria towards sources of chemical attractants. Although this system relaxes to a steady-state in response to environmental changes, the signalling events within the chemotaxis network are noisy and cause large temporal variations of the motor behaviour even in the absence of stimulus<sup>3</sup>. The fact that the same signalling network governs both behavioural variability and cellular response raises the question of whether these two traits are independent. Here, we experimentally establish a fluctuation-response relationship in the chemotaxis system of living bacteria. Using this relationship, we demonstrate the possibility of inferring the cellular response from the behavioural variability measured before stimulus. In monitoring pre- and post-stimulus switching behaviour of individual bacterial motors, we found that variability scales linearly with the response time for different functioning states of the cell. This study highlights that the fundamental fluctuation-response relationship is not constrained to physical systems at thermodynamic equilibrium<sup>4</sup> but is extensible to living cells<sup>5</sup>. Such a relationship not only implies that behavioural variability and cellular response are coupled traits, but also provides a general framework to examine how the selection of a network design shapes this interdependence.

---

It is standard to characterize the stochastic dynamics of physical systems in thermodynamic equilibrium by measuring spontaneous fluctuations and responses to small external perturbations. Because these two distinct measurements contain the same information, they are related by the fluctuation-dissipation theorem (FDT)<sup>4</sup>. Although the FDT has practical applications to evaluate force-extension sensors for single bio-molecules<sup>6–7</sup> and to predict static cell-to-cell variability of gene expression<sup>8–9</sup>, it has not been possible to apply it directly to study the dynamical behaviour of living cells because these cells are open systems with significant non-thermal dynamics. However, this theorem has recently been extended to a fluctuation-response theorem (FRT) for systems that are out of thermodynamic equilibrium, when the systems have a well-defined steady state and Markovian dynamics<sup>5,10–12</sup>. For application to living cells this condition amounts to

studying dynamic processes with sufficiently short “memory” that they can relax to a well-defined steady state. We wish to employ the FRT as an operational framework to establish the interdependence of distinct cellular traits without relying on the biochemical details of a specific signalling pathway. A fundamental open question is whether fluctuations and responses of living cells are ever related by the FRT.

To tackle this question experimentally, we used the well-characterized chemotaxis system in *E. coli*, which governs bacterial locomotion<sup>13</sup>. This bacterial system displays both strong fluctuations and adaptive responses to external stimuli. Additionally, it exhibits reproducible relaxation to steady states on timescales much shorter than the cell’s lifetime. In this system, noise amplitude and adaptive response are both governed by the same signalling pathway. Therefore, it is plausible that they are dynamically coupled in the manner specified by the FRT. Cell dynamics sensitive to intracellular noise are likely to be similarly sensitive to small extra-cellular perturbations, such as sudden changes in the environment.

The chemotaxis network is a phosphoryl cascade that controls the concentration of the phosphorylated form of the signalling protein CheY<sup>1-2</sup>. Its active form, CheY-P, binds to the sensory basal part of the flagella rotary motor and induces clockwise (CW) rotation, causing tumbling that randomizes the bacterial swimming direction. In response to a sudden step of attractant concentration, the CW bias (the probability for the motor to rotate clockwise) decreases with [CheY-P], and bacteria tumble less frequently. Therefore, in swimming bacteria, chemotaxis is achieved by changing the length of the runs between tumbles in response to the environment. One of the hallmarks of bacterial chemotaxis is adaptation. Following a stepwise stimulus, the CW bias decreases abruptly, before slowly adapting back to its pre-stimulus level. Even when bacteria are adapted to their environment, the CW bias of individual cells fluctuates around the mean. These temporal fluctuations in CW bias reflect slow fluctuations in signalling events throughout the transduction network<sup>14</sup>. To verify that the bacterial chemotaxis system satisfies the FRT, we monitored both the temporal fluctuations of the CW bias before stimulus and the cellular response to a small stimulus at the single-cell level. Both quantities were obtained from the time series of CW and CCW intervals of individual motors from bacteria immobilized onto a glass coverslip<sup>15</sup> and submerged in a motility medium that does not support growth. Single-cell experiments are complicated by inherent cell-to-cell differences in relative chemotaxis protein concentration, leading to differences in switching dynamics (Fig. 1a). To compare cells with similar behaviour, we sorted wild-type cells according to their steady-state CW bias (Methods). These CW bias bins define different classes of cells, which, despite being genetically identical, have different dynamics and must be analyzed separately<sup>3</sup>.

First, we quantified the response in single cells by measuring the length of successive CCW intervals immediately following the stimulus. The small stimulus (10 nM of aspartate) used in this study is close to the limit of sensitivity of the bacterial chemotaxis system<sup>16</sup>. We found that the length of the CCW intervals after stimulus was only slightly longer than that in pre-stimulus cells (Fig. 1b). Therefore, we expected the response of the system to be within the linear regime, which was necessary to apply the FRT. We also tested the response of the chemotaxis system for a stimulus 100 times larger (1  $\mu$ M aspartate). At the single-cell level, the length of first CCW interval following the small stimulus (Supplementary Fig. 1a) was distributed around the mean CCW interval length before stimulus (Supplementary Fig. 1b). Given that CCW interval length is a stochastic variable, we averaged the CCW interval lengths after stimulus between cells and found that the length of first CCW interval was slightly longer than the pre-stimulus length (Fig. 1b). Surprisingly, the second CCW interval following the stimulus returned to near pre-stimulus lengths for both large and small attractant concentrations (Fig. 1c and Supplementary Fig. 1c for individual cells). Although the cellular response to stimulus spreads in some cases beyond the second interval

(Supplementary Fig. 1d–e), these results qualitatively indicate that the first interval contains most of the chemotactic response to both small and large stimuli.

To characterize the system quantitatively, we defined the response time as the cumulative length of post-stimulus CCW intervals that are strictly longer than the mean CCW interval length before stimulus (Fig. 1b–c and Supplementary Fig. 1e). This procedure is not exact but it yields a realistic estimate of the response time under the condition of small stimulus (Supplementary Fig. 2). We found that the response time decreased with CW bias for both small (Fig. 2a) and large stimuli (Fig. 2a, inset). Because all cells returned to their pre-stimulus behaviour (Supplementary Fig. 1), the system exhibited near-precise adaptation at the single-cell level, regardless of CW bias (Supplementary Fig. 3 for each CW bias bin and for individual cells). This result is concordant with that obtained from population measurements<sup>17–18</sup> and shows that the dynamics have sufficiently short “memory” that they can relax to a well-defined steady-state.

A direct consequence of the linear approximation is that the response time of the system to a small external stimulus should be proportional to the correlation time of the spontaneous fluctuations before stimulus. Using serial correlation analysis<sup>19–20</sup>, we evaluated the correlation time in non-stimulated cells (Supplementary Fig. 4). In agreement with our assumption of linear dynamics<sup>21</sup> and the general prediction of the FRT, we found that the correlation time scales linearly with the response only to small stimulus ( $R^2=0.75$ ; Fig. 2b) whereas to large stimulus it scales poorly with regression coefficient  $R^2=0.07$  (Fig. 2b, inset). This result has an important practical implication: The response time that governs the cellular response in chemotaxis can be experimentally inferred by measuring the temporal correlations in behavioural fluctuations from cells before stimulus.

Cellular behavioural variability can also be defined by the amplitude of the noise rather than its temporal correlations. To characterize the amplitude of the output noise of the chemotaxis network, we computed the power spectral density of the switching binary time series measured from individual motors before stimulus (Fig. 3a, inset for CW bias bin 0.15–0.20. See Supplementary Fig. 5 for all CW bias). We evaluated the low frequency noise by integrating the power spectrum between  $f = 1/1500 \text{ s}^{-1}$  and  $f = 1/10 \text{ s}^{-1}$ . In this frequency range, the temporal fluctuations are putatively caused by the slow methylation-demethylation of the receptor-kinase complexes that are also controlling the adaptive process<sup>14</sup>. Two elements contribute to the observed output noise: i) the spontaneous noise associated with the signalling events of the chemotaxis network and ii) the stochastic switching behaviour of the bacterial motor (Fig. 3a). The binary nature of the switching behaviour of the motor dominates the variance of the noise and masks the signalling noise within the chemotaxis network. Therefore, using a procedure developed by Shibata et al.<sup>22</sup>, we decoupled the signalling noise,  $\sigma^2_{\text{CheYp}}$ , from that of the motor. We then found that the signalling noise decreased with the CW bias (Fig. 3b).

Operationally, we used a simplified expression of the FRT, where the response function of the chemotaxis system  $\mu(t)$  and the autocorrelation function  $C(t)$  of the spontaneous

fluctuations of the cellular behaviour should be related by  $\mu(t) = -K \frac{d}{dt} C(t)$ . Here, the fluctuation-response coupling parameter  $K$  is a constant that may depend on the genetic background, growth conditions, and functional state of the cell. We plotted the Fourier

transform of the coefficient  $\left| \tilde{K}(\omega) \right|_{\text{CW bias}} = \frac{1}{\omega} \frac{|\tilde{\mu}(\omega)|}{|\tilde{C}(\omega)|}$  as a function of CW bias. We found that the coupling  $K$  was indeed constant for CW bias ranging from ~0.05 to 0.5 (~0.1 to 0.3 for a large stimulus, albeit at a different value) and for frequencies ranging from 1 s to 5 min (10 s to 5 min for a large stimulus) (Fig. 4a, Supplementary Fig. 6 for  $|\mu(\omega)|$ , and Supplementary

Fig. 7 for the inverse of  $|\tilde{K}(\omega)|_{CW\ bias}$ ). The finding that  $|\tilde{K}(\omega)|_{CW\ bias}$  is constant for small stimulus indicates that the FRT is applicable to the chemotaxis system over a wide range of intracellular parameters. In the most general non-equilibrium case, the coupling  $K$  may change when the genetic background or the growth conditions are modified. On the other hand, we found that the value of  $|\tilde{K}(\omega)|_{CW\ bias}$  was similar across a wide range of CW biases, reflecting that the coupling constant is independent from the functioning states of the cell and levels of expression of the chemotaxis proteins. This result is remarkable since most of the chemotaxis network has highly non-linear signal processing, such as the cooperative behaviour between receptors that governs the input-output relationship of the receptor-kinase complex and the signalling cascade that involves phosphorylation/dephosphorylation cycles in series<sup>23–24</sup>.

The standard assumption is to consider that noise is a limiting factor in intracellular signalling and that evolution selects network designs against it<sup>25</sup>. Using the framework of the FRT, we asked whether the temporal fluctuations in the switching rate of the motor and cellular response are ever dynamically coupled. In such a situation, it would not be possible to reduce the noise in the network output without affecting the cellular response itself. Remarkably, we found that the response time to a small external stimulus scaled linearly with the signalling noise from the chemotaxis network in cells before stimulus ( $R^2=0.8$ ; Fig. 4b), which was consequently linearly related to the correlation time ( $R^2=0.9$ ; Fig. 4c). Furthermore, we found that the response time to a large stimulus scaled poorly ( $R^2=0.4$ ) with the signalling noise, reflecting that for large stimulus, the system operates outside the regime of linear approximation (Fig. 4b, inset).

We interpret this observation in simple mathematical terms, where the fluctuations in the network output,  $\delta CheYp$ , about its average have linearized kinetics of the form of a

Langevin equation  $\frac{d}{dt}\delta CheYp = -\frac{1}{\tau}\delta CheYp + \sqrt{D}\delta(t)$ <sup>21,26</sup>, where  $\sqrt{D}\delta(t)$  is an input random function that has the characteristics of white noise and an amplitude  $D$ , and  $\tau$  is the measured correlation time in the output of the signalling system. In this coarse-grained picture, there

should exist a strict relationship between the output noise amplitude,  $\sigma_{CheYp}^2$  and the

correlation time of the system,  $\tau$ , where  $\sigma_{CheYp}^2 = \frac{D}{2}\tau$ . Although the coefficient  $D$  can depend on intracellular parameters in a complex way, our experiments surprisingly showed that two

cellular traits, the amplitude of the output noise  $\sigma_{CheYp}^2$  and the cellular response time are linearly coupled. This observation implies that the coefficient  $D$  remains approximately constant over a wide range of functioning states of the cell (i.e. CW bias). While the FRT predicts the existence of a coupling between cellular response and noise, it does not specify how this coupling depends on the different states of the cell. Interestingly, the observed linear coupling implies that the coefficient  $D$  remains nearly constant with the functioning states of the cell (expression levels of chemotaxis proteins or CW biases). We hypothesize that the specific design of the signalling pathways itself could govern such a constraint. We find that a simple kinetic model and experimental data support this hypothesis (Supplementary Fig. 8): the value of the coefficient  $D$  is governed by the adaptation mechanism that uses the classic futile cycle<sup>27</sup> as a core module where two antagonistic enzymes regulate the activity of the kinase-receptor complexes. Since the futile cycle is a design shared by a large class of signalling pathways<sup>21,28–29</sup>, it raises the possibility that for these systems as well, noise and cellular response are coupled in a similar way. More generally, to gain further insights on the nature of this coupling, future experiments should examine the role of specific designs of signalling network on this interdependence<sup>27</sup>.

In conclusion, we experimentally established that the cellular response to a small external stimulus can be inferred by characterizing the signalling noise before the stimulus. Consequently, we anticipate that below an upper bound imposed by rotational diffusion<sup>28</sup>, cells with the largest behavioural variability before stimulus would also exhibit the strongest chemotactic drift in response to an external stimulus, as theoretically discussed in a full kinetic model in ref. 21. The fact that the distribution of wild-type cells peaks for the phenotype with the largest behavioural variability might lead one to conclude that noise may be a key trait that has been independently selected<sup>14</sup>. Instead, the FRT indicates that behavioural variability and cellular response are profoundly coupled; these two traits cannot be adjusted independently by varying the levels of gene expression alone. This work illustrates the significance of the FRT as an operational framework that uses first principles rather than specific molecular details to establish a fundamental relationship between dynamical properties of signalling networks in living cells.

## Methods Summary

### Bacterial strains and plasmids

**RP437 strain**—We used RP437 as wild-type *E. coli* strain<sup>29</sup>. We transformed the strain with the TetR-inducible plasmid pZE21-CheR that encoded CheR.

**Behavioural assays**—Cultures grew overnight in 3 mL of tryptone broth at 35°C with shaking at 200 rpm. Then we transferred the overnight cultures to a 250 mL flask, where we diluted them 1:50 in 12 mL tryptone broth and grew the cells again at 35°C at 200 rpm. To obtain cultures with different CW biases, we induced plasmid expression with various concentrations of anhydrotetracycline (aTc) in the diluted overnight cultures. The media also contained the antibiotic specific to each plasmid. We harvested the cells when the optical density (O.D.) reached ~0.3 at 600 nm. We washed the cells and resuspended them in motility medium (0.1 mM EDTA, 0.1 mM L-methionine, 10 mM potassium phosphate pH 7.0). Photo-release of caged-aspartate: We illuminated the sample with an intense UV light from the Xenon flash coupled into a light guide (A2873, Quartz glass fiber, Hamamatsu) and widely focused onto the whole sample with two lenses (UV coated lenses, focal = 35 mm, diameter = 25.4 mm; focal = 20 mm, diameter = 12.7 mm, ThorLabs Inc.). These UV flashes produced a stepwise release of 1  $\mu$ M L-aspartate from the 0.5 mM (or 10 nM L-aspartate from the 5  $\mu$ M) caged L-aspartate<sup>30</sup>.

**Binning scheme of CW biases**—To obtain cultures with different CW biases, we induced plasmid expression with various concentrations of anhydrotetracycline (aTc) (0–2.5 ng/mL). We sorted cells by their CW bias before stimulus and grouped them into the following CW bias intervals: 0.00–0.05 (a), 0.05–0.10 (b), 0.10–0.15 (c), 0.15–0.20 (d), 0.20–0.25 (e), 0.25–0.30 (f), 0.30–0.40 (g), 0.40–0.50 (h) and 0.50–0.60 (i). We observed that most wild-type (RP437) *E. coli* cells had CW biases between 0.05 and 0.2 (Fig. 1a). To increase the chance to obtain cells with CW bias higher than 0.2, we transformed wild-type cells with the TetR-inducible plasmid pZE21-CheR that encodes CheR. The wild-type cells with and without plasmid exhibited the similar noise (Fig. 3a) and a response time (Supplementary Fig. 1a, c, and d) at the single cell level.

**Cellular Response**—For each CW bias bin, the response time was measured from the time of stimulus through all successive averaged CCW intervals that were different in duration from the mean CCW interval before stimulus. CW intervals between successive CCW intervals were also included to compute the response time. Although the cellular response to stimulus stretches, in some cases, beyond the second interval, the first interval contained most of the chemotactic response to both small and large stimuli.

**Correlation time**—Because autocorrelation functions of time series of CW and CCW switching events did not exhibit a clear typical correlation time (Supplementary Fig. 4a) we used a serial correlation analysis. The serial correlation coefficients (Supplementary Fig. 4b) for the CCW interval lengths allow us to determine how long the CCW sequences are correlated<sup>19–20</sup>. We converted the correlated number of sequences to the real correlation time lengths, including the half-length of the first uncorrelated CCW interval. To determine if the sequences in each lag (the number of preceding CCW intervals) were correlated, we used the Wilcoxon rank sum test (“ranksum” Matlab function) at a significance level of  $p = 0.01$  as in ref. 20. We considered the first non-zero lag that had  $h = 0$  as the end of the correlation. For the Wilcoxon rank sum test in each CW bias bin, we used 100 consecutive CCW and CW interval lengths and 300 randomly reshuffled series. We performed the Wilcoxon rank sum test 100 times with the different sets of reshuffled series and determined the average correlated lags and the average correlation time in each CW bias bin (Supplementary Fig. 4c).

**Low frequency noise and motor noise**—We define the low frequency noise ( $Noise_i^{LF}$ ) of  $i^{\text{th}}$  cell as the integrated power density ( $P_i(f)$ ) of the binary time series from  $f_i = 1/1500$

$s^{-1}$  to  $f_f = 1/10 s^{-1}$   $Noise_i^{LF} \equiv \int_{f_i}^{f_f} P_i(f) \cdot df$  (Fig. 3a). The integrated flat baseline of the power density (Fig 3a, dark grey line) in the same time scale defines the low frequency motor noise ( $Noise_i^{LF, Motor}$ ). We estimated signalling noise from the average experimental power spectral density, the average CW bias ( $\overline{M^*}$ ), and the gain function ( $g_M$ ) between the input signal (steady level ( $\overline{Y_p}$ ) of [CheY-P]) and output signal (CW bias  $\equiv \overline{M^*}$ ) using the

formula  $\sigma_{M,T}^2 \cong \sigma_M^2 + g_M^2 \overline{M^*}^2 \frac{\sigma_{CheYp}^2}{\overline{Y_p}^2}$  introduced by Shibata et al.<sup>22</sup> (Full Methods).

**Full Methods** and any associated references are available in the online version of the paper located at [www.nature.com/nature](http://www.nature.com/nature).

## Full Methods

### Strains and Plasmids

**RP437 strain**—RP437 is a wild-type *E. coli* strain for chemotaxis<sup>29</sup>. To construct pZE21-CheR, we PCR amplified the *cheR* the *E. coli* RP437 chromosome with the following primers: CheR-KpnI-5': 5'-gcc ggt acc atg act tea tca tct ctg ccc tg-3' and CheR-HindIII-3': 5'-cgc aag ctt tta atc ctt act tag cgc at-3'. The gene fragment was inserted in the KpnI and HindIII sites of a pZE21 series plasmid<sup>31</sup> that contained a kanamycin resistance cassette and a TetR inducible promoter. The plasmid pUHS-IntI encodes *tetR* under a constitutive promoter, which modulates the expression of the TetR-regulated *cheR* construct. This plasmid carries a spectinomycin resistance gene.

**RP4972 strain**—RP4972 is derived from the RP437 strain and contains a deletion of the *cheB* gene (gift from J.S. Parkinson). RP4972 cells were complemented with a Lac-inducible plasmid, pME304, expressing CheBc proteins<sup>32</sup>.

**RP4992 strain**—RP4992 is derived from the RP437 strain and contains a deletion of *cheB* gene (gift from J.S. Parkinson). RP4992 cells were complemented with a LacR-inducible plasmid, pZA32-CheBc, and a TetR-inducible plasmid, pZA21-CheBc, both expressing CheBc proteins. To construct pZA32-CheBc, we amplified the *cheBc* gene fragment from the chromosome of *E. coli* RP437 cells with primers CheBc-5': gcg gta ccg cat gct gaa ggc

*ggg gcc gtt gtt g* and XbaI-CheB-3': *gct cta gat taa ata cgt atc gcc tgt c*. The gene fragment was inserted in the KpnI and XbaI sites of a pZA32 series plasmid that contained a chloramphenicol resistant cassette and a LacR inducible promoter. To construct pZA21-CheBc, we amplified the *cheBc* gene fragment from the chromosome of *E. coli* RP437 cells using the primers CheBc-5' and XbaI-CheB-3'. We inserted the gene fragment into the KpnI and XbaI sites of a pZA21 series plasmid that contained a kanamycin resistant cassette and a TetR inducible promoter.

### HPLC calibration of the release of aspartate

We prepared 10  $\mu$ L samples of 0.5 mM caged L-aspartate solution under the same conditions for the chemotaxis experiments and illuminated them with intense UV light from a Xenon flash lamp (built-in L7685 reflective mirror, 60W, Hamamatsu). We estimated the relative concentration of the caged L-aspartate in each sample by the HPLC peak area. By comparing the decreasing HPLC peak area with its initial peak area, we found the released L-aspartate concentration as a function of the number of UV flashes (Supplementary Fig. 9). The samples released about 1  $\mu$ M L-aspartate per UV flash. The HPLC gradient conditions had five steps: i) equilibrium with 20% acetonitrile, 0.1% TFA/80% water, 0.1% TFA; ii) gradient of 20–55% acetonitrile over 30 min; iii) washing-1 with 55–90% acetonitrile over 20 min; iv) washing-2 with 90% acetonitrile for 5 min; and v) equilibrium with 20% acetonitrile, 0.1% TFA/80% water, 0.1% TFA.

### Photo-release and single cell assay

We sheared the flagella of the cells by slowly forcing them through a thin needle (inner diameter = 0.19 mm, 27 G  $\frac{1}{2}$ , B–D) 40 times. We washed the cells and resuspended them in motility medium. We prepared poly-L-lysine coated glass slides (No. 1 $\frac{1}{2}$ , 18 mm, Corning) and a solution of beads (Polybead Amino 1.0 micron Microspheres, Polysciences, Inc.) coated with rabbit antibodies against flagella. We mixed the cells (4–5  $\mu$ L) with the beads (4–5  $\mu$ L) and incubated them for 20 min at room temperature. This process caused the cell bodies to stick to the glass slide and the beads to attach to the flagella. Although the probability for a bead to attach to a rotating flagellum was low, we consistently obtained a few labelled flagella in each sample. After incubation we removed the unattached cells and beads and then added 8  $\mu$ L of 5  $\mu$ M (for small stimulus) or 500  $\mu$ M (for large stimulus) caged L-aspartate solution to the sample medium. We covered the sample with oil (Immersion oil transparent to UV: type FF, Cargille Laboratories Inc.) to prevent evaporation. We placed the sample under a dark field condenser to produce a bright red image of the bead. Harmful blue light was filtered out by a long-pass filter (NT52-543, Edmund Industrial Optics). We observed the samples under an Olympus IX71 microscope with an oil immersion objective 100 $\times$  (numerical aperture = 1.3, Olympus Uplan FI, oil iris  $\infty/0.17$ , Japan). We recorded the long circular motions of individual beads attached to rotating flagella of single cells through a 4-quadrant photomultiplier (PMT) (Type: R5900U-01-M4, Hamamatsu). The signal from the PMT, a 4 voltage time series, was monitored with a PC computer via LabView software (National Instrument, Austin, TX). The rotation of the bead was simultaneously recorded using a CCD camera (1/3" midresolution Exview digital B/W camera, Sony). We converted the signal to a binary time series indicating transitions between CCW and CW rotations. After 1500 s (or 300 s) of recording the rotational motion of the bead, we photo-released the caged aspartate (caged L-Aspartic Acid, Sodium Salt (189110): N-[1-(2-Nitrophenyl)ethyloxycarbonyl]aspartic Acid, Sodium, M.F. (C<sub>13</sub>H<sub>13</sub>N<sub>2</sub>O<sub>8</sub>·Na), M.W. (348.2),  $\lambda_{\max}$  (264 nm),  $\epsilon$  (4,710 M<sup>-1</sup> cm<sup>-1</sup>), Calbiochem or synthesized by David Trentham, Gordon Reid, and John Corrie) (Supplementary Fig. 9). The magnitude of the stepwise stimulus corresponds to the typical increase in attractant concentration encountered by bacteria swimming in a gradient of 1 nM/ $\mu$ m ref<sup>34–35</sup>.

## Definition of CW bias

We define the CW bias ( $b_{i,j}$ ) of the  $i^{\text{th}}$  cell at the  $j^{\text{th}}$  CW interval ( $T_{i,j}^{\text{CW}}$ ) as the ratio between the duration of the  $j^{\text{th}}$  CW interval and the sum of the  $j^{\text{th}}$  CW interval and  $j^{\text{th}}$  counter-

clockwise (CCW) interval ( $T_{i,j}^{\text{CCW}}$ ):  $b_{i,j} = \frac{T_{i,j}^{\text{CW}}}{T_{i,j}^{\text{CCW}} + T_{i,j}^{\text{CW}}}$ . We calculated the pre-stimulus CW bias of the  $i^{\text{th}}$  cell ( $\langle b_{i,j} \rangle_{j^{\text{before}}}$ ) over a 1500-second (or 300-second) time series of  $j_{\text{max}}^{\text{before}}$  CCW and

$j_{\text{max}}^{\text{before}}$  CW intervals before stimulus as  $\langle b_{i,j} \rangle_{j^{\text{before}}} = \frac{\sum_{j=1}^{j_{\text{max}}^{\text{before}}} T_{i,j}^{\text{CW}}}{t_{i,j_{\text{max}}^{\text{before}}} - t_{i,j_{\text{max}}^{\text{before}}-2}} \approx 1500$  seconds for the cells responding to the small stimulus,  $t_{i,j_{\text{max}}^{\text{before}}} \approx 1500$  seconds for cells responding to the large stimulus with CW bias  $< 0.25$  and  $t_{i,j_{\text{max}}^{\text{before}}} \approx 300$  seconds for cells responding to the large stimulus with CW bias  $\geq 0.25$ ). To calculate the post-stimulus CW bias of the  $i^{\text{th}}$  cell ( $\langle b_{i,j} \rangle_{j^{\text{after}}}$ ), we took the temporal average of the  $b_{i,j}$  over a 1500-second time series after a

small stimulus following the cell's response:  $\langle b_{i,j} \rangle_{j^{\text{after}}} = \frac{\sum_{j=j_S+3}^{j_{\text{max}}} T_{i,j}^{\text{CW}}}{t_{i,j_{\text{max}}} - t_{i,j_S} + 2}$ . Here,  $j_S+k$  represents the  $k^{\text{th}}$  interval after the stimulus (at  $j=j_S$ ) and  $t_{i,j_{\text{max}}} - t_{i,j_S+2} \approx 1500$ sec. To prevent overshooting the time regime seen after the response to a large stimulus, we did not include

the first 200 CCW and CW interval pairs after the stimulus:  $\langle b_{i,j} \rangle_{j^{\text{after}}} = \frac{\sum_{j=j_S+201}^{j_{\text{max}}} T_{i,j}^{\text{CW}}}{t_{i,j_{\text{max}}} - t_{i,j_S+200}}$ , where  $t_{i,j_{\text{max}}} - t_{i,j_S+2} \approx 900$  sec (for the cells with CW bias  $< 0.25$ ) or  $t_{i,j_{\text{max}}} - t_{i,j_S+2} \approx 300$  sec (for the cells with CW bias  $\geq 0.25$ ).

## Cellular Response

Intervals were strictly different when the associated standard error of the mean CCW intervals after stimulus did not overlap with the mean pre-stimulus CCW interval (dark grey dotted lines in Fig. 1b and 1c, and Supplementary Fig. 1e). In some instances, the response time included the second (and first CW) and/or third CCW (and second CW) interval after stimulus. Because of the presence of a few outliers, we used the geometric mean to compute the average of the CCW interval lengths after stimulus for each CW bias bin (Fig. 1b).

## Estimating signalling noise

To estimate the signalling noise, we used a formula  $\sigma_{M,T}^2 \cong \sigma_M^2 + g_M^2 \overline{M}^2 \frac{\sigma_{\text{CheYp}}^2}{\overline{Y}_P^2}$  which shows

the relationship between the variance ( $\sigma_{\text{CheYp}}^2$ ) of [CheY-P] and the variance ( $\sigma_{M,T}^2$ ) of the output signals. This formula was derived from a model recently introduced to describe generally the gain-noise relationship between the input and output signals in the chemical reaction network<sup>22</sup>. As Shibata et al. showed<sup>22</sup>, the temporally fluctuating output signal from a well defined steady state (CW bias) due to the fluctuating input signal ([CheY-P]) is described by the following linearized chemical Langevin equation,  $\delta \dot{M}^* = \gamma_M \delta Y_P - \delta M^* / \tau_M + \xi_M(t)$ , where  $\delta M^*$  and  $\delta Y_P$  are small deviations of the CW bias and the CheY-P

concentration from their steady values, respectively, and  $\tau_M$  and  $\xi_M(t)$  are the typical time scale of the motor alone and the Gaussian white noise term which satisfies  $\overline{\xi_M(t)}=0$  and  $\overline{\xi_M(t) \cdot \xi_M(t')}=\sigma_{\xi_M}^2 \cdot \delta(t-t')$ , respectively. From this equation, we obtain the total variance of the output signals due to the temporally fluctuating input signals and the

Gaussian white noise:  $\sigma_{M,T}^2 = \frac{g_M \overline{M^*}}{\Theta_M} + g_M^2 \overline{M^*}^2 \frac{\tau_{CheYp}}{\tau_M + \tau_{CheYp}} \frac{\sigma_{CheYp}^2}{\overline{Y_p}^2}$ , where  $\overline{Y_p}$  is the steady value of

fluctuating CheY-P concentrations given by  $\overline{Y_p} = K_M \cdot \left( \frac{\overline{M^*}}{1 - \overline{M^*}} \right)^{1/N_H}$  ( $K_M$  and  $N_H$  (Hill coefficient) are given by respectively 3.1  $\mu\text{M}$  and 10.3 in ref.<sup>15</sup>), the constant  $\Theta_M$  in the first term is defined by  $\Theta_M \equiv 2g_M \overline{Y_p} / \sigma_{\xi_M}^2$ ,  $\overline{M^*}$  is the CW bias,  $g_M$  is the gain function defined as the ratio of the fractional change of the output signal to the input signal (i.e.

$g_M = (\delta M^* / \overline{M^*}) / (\delta Y_p / \overline{Y_p}) = N_H \cdot (1 - \overline{M^*})$ ). The last form is obtained from the ref.<sup>15</sup>), and  $\tau_{CheYp}$  is a characteristic time scale of the [CheY-P] fluctuations and is proportional to the

input noise ( $\sigma_{CheYp}^2$ ):  $\tau_{CheYp} = \frac{\sigma_{\xi_Y}^2}{2} \cdot \sigma_{CheYp}^2$ . This relationship is derived from the chemical Langevin equation describing the [CheY-P] fluctuations from its steady state

$(\overline{Y_p}) : \delta \dot{Y_p} = - \frac{\delta Y_p}{\tau_{CheYp}} + \xi_Y(t)$ , where  $\xi_Y(t)$  is a Gaussian white noise term which satisfies

$\overline{\xi_Y(t)}=0$  and  $\overline{\xi_Y(t) \cdot \xi_Y(t')}=\sigma_{\xi_Y}^2 \cdot \delta(t-t')$ . As long as the external stimulus is small enough, the response time to the stimulus should scale to  $\tau_{CheYp}$ . For the broad range of the functioning states of this paper, we have one condition,  $\tau_{CheYp} \gg \tau_M$ , in timescales involved in this system. Under this condition, the above formula for the total variance of the output signals

can be simplified to  $\sigma_{M,T}^2 \cong \sigma_M^2 + g_M^2 \overline{M^*}^2 \frac{\sigma_{CheYp}^2}{\overline{Y_p}^2}$ , where  $\sigma_{M,T}^2$  is given by  $\overline{M^*} \cdot (1 - \overline{M^*})$  for any binary time series and is equal to the integral of the power spectral density over all frequencies (Supplementary Fig. 5: black) averaged over all wild-type (RP437 and RP437 expressing CheR from pZE21-CheR) cells and  $\sigma_M^2$  is equal to the integral of the power density (Supplementary Fig. 5: dark grey line) of the isolated motor. We approximated the baseline of the motor power density by finding the mean value of the flat regime (from  $f_i=1/10 \text{ s}^{-1}$  to  $f_f=1/5 \text{ s}^{-1}$ ) of the average experimental power density and extending the baseline to the lowest frequency. By using the simplified formula above, we estimated the signalling noise ( $\sigma_{CheYp}^2$ ) values in each CW bias bin (Fig. 3b).

## Definition of noise

We hypothesize that a small number of proteins and thermally activated biochemical reaction rates cause stochastic fluctuations between functional states of signalling proteins. Operationally, we monitor the cellular behaviour in a motility medium that does not support growth but allows bacteria to perform chemotaxis. Under these conditions, the observed noise does not result from protein synthesis or degradation; rather, it results from fluctuations in protein functional states about a well-defined steady state.

## Supplementary Material

Refer to Web version on PubMed Central for supplementary material.

## Acknowledgments

This research was funded by NSF DMR award 0213745 to MRSEC at the University of Chicago, and NIH award R01AI059195-03 to PC. WP and TE were supported by an Alfred P. Sloan Research Fellowship and a National Academies Keck Futures Initiative to TE. David Trentham supplied caged L-aspartate. JFM was supported by NSF awards PHY-0852130 and DMR-0715099 and NIH grant 1U54CA143869-01. This work was also supported by the Chicago Biomedical Consortium with support from The Searle Funds at The Chicago Community Trust. We thank T. Shimizu for discussions and sharing unpublished work. We thank Jeff Moffitt and Kevin Wood for comments on the manuscript and all members of the Cluzel lab for many helpful discussions. Wendy Grus provided editorial assistance.

## References

1. Bourret RB, Borkovich KA, Simon MI. Signal transduction pathways involving protein phosphorylation in prokaryotes. *Annu Rev Biochem.* 1991; 60:401–441. [PubMed: 1883200]
2. Bourret RB, Stock AM. Molecular information processing: Lessons from bacterial chemotaxis. *J Biol Chem.* 2002; 277:9625–9628. [PubMed: 11779877]
3. Korobkova EA, Emonet T, Park H, Cluzel P. Hidden stochastic nature of a single bacterial motor. *Phys Rev Lett.* 2006; 96 058105.
4. Callen HB, Welton TA. Irreversibility and Generalized Noise. *Phys Rev.* 1951; 83:34–40.
5. Prost J, Joanny JF, Parrondo JM. Generalized fluctuation-dissipation theorem for steady-state systems. *Phys Rev Lett.* 2009; 103 090601.
6. Bustamante C, Macosko JC, Wuite GJL. Grabbing the cat by the tail: Manipulating molecules one by one. *Nat Rev Mol Cell Bio.* 2000; 1:130–136. [PubMed: 11253365]
7. Dornigac J, Kalinowski A, Erramilli S, Mohanty P. Dynamical response of nanomechanical oscillators in immiscible viscous fluid for in vitro biomolecular recognition. *Phys Rev Lett.* 2006; 96
8. Paulsson J. Summing up the noise in gene networks. *Nature.* 2004; 427:415–418. [PubMed: 14749823]
9. Ozbudak EM, Thattai M, Kurtser I, Grossman AD, van Oudenaarden A. Regulation of noise in the expression of a single gene. *Nat Genet.* 2002; 31:69–73. [PubMed: 11967532]
10. Cugliandolo LF, Dean DS, Kurchan J. Fluctuation-dissipation theorems and entropy production in relaxational systems. *Phys Rev Lett.* 1997; 79:2168–2171.
11. Chetrite R, Falkovich G, Gawedzki K. Fluctuation relations in simple examples of non-equilibrium steady states. *J Stat Mech-Theory E.* 2008
12. Speck T, Seifert U. Restoring a fluctuation-dissipation theorem in a nonequilibrium steady state. *Europhys Lett.* 2006; 74:391–396.
13. Berg HC. Motile behavior of bacteria. *Physics Today.* 2000; 53:24–29.
14. Korobkova E, Emonet T, Vilar JM, Shimizu TS, Cluzel P. From molecular noise to behavioural variability in a single bacterium. *Nature.* 2004; 428:574–578. [PubMed: 15058306]
15. Cluzel P, Surette M, Leibler S. An ultrasensitive bacterial motor revealed by monitoring signaling proteins in single cells. *Science.* 2000; 287:1652–1655. [PubMed: 10698740]
16. Sourjik V, Berg HC. Receptor sensitivity in bacterial chemotaxis. *Proc Natl Acad Sci U S A.* 2002; 99:123–127. [PubMed: 11742065]
17. Barkai N, Leibler S. Robustness in simple biochemical networks. *Nature.* 1997; 387:913–917. [PubMed: 9202124]
18. Alon U, Surette MG, Barkai N, Leibler S. Robustness in bacterial chemotaxis. *Nature.* 1999; 397:168–171. [PubMed: 9923680]
19. Anderson RL. Distribution of the serial correlation coefficient. *Ann Math Stat.* 1942; 13:1–13.
20. Ratnam R, Nelson ME. Nonrenewal statistics of electrosensory afferent spike trains: implications for the detection of weak sensory signals. *J Neurosci.* 2000; 20:6672–6683. [PubMed: 10964972]
21. Emonet T, Cluzel P. Relationship between cellular response and behavioral variability in bacterial chemotaxis. *Proc Natl Acad Sci U S A.* 2008; 105:3304–3309. [PubMed: 18299569]

22. Shibata T, Fujimoto K. Noisy signal amplification in ultrasensitive signal transduction. *Proc Natl Acad Sci U S A*. 2005; 102:331–336. [PubMed: 15625116]
23. Bray D, Levin MD, Morton-Firth CJ. Receptor clustering as a cellular mechanism to control sensitivity. *Nature*. 1998; 393:85–88. [PubMed: 9590695]
24. Sourjik V, Berg HC. Functional interactions between receptors in bacterial chemotaxis. *Nature*. 2004; 428:437–441. [PubMed: 15042093]
25. Rao CV, Wolf DM, Arkin AP. Control, exploitation and tolerance of intracellular noise. *Nature*. 2002; 420:231–237. [PubMed: 12432408]
26. Bialek W, Setayeshgar S. Physical limits to biochemical signaling. *Proc Natl Acad Sci U S A*. 2005; 102:10040–10045. [PubMed: 16006514]
27. Shinar G, Feinberg M. Structural Sources of Robustness in Biochemical Reaction Networks. *Science*. 2010; 327:1389–1391. [PubMed: 20223989]
28. Andrews BW, Yi TM, Iglesias PA. Optimal noise filtering in the chemotactic response of *Escherichia coli*. *PLoS Comput Biol*. 2006; 2:e154. [PubMed: 17112312]
29. Parkinson JS, Houts SE. Isolation and behavior of *Escherichia coli* deletion mutants lacking chemotaxis functions. *J Bacteriol*. 1982; 151:106–113. [PubMed: 7045071]
30. Jasuja R, Yu-Lin, Trentham DR, Khan S. Response tuning in bacterial chemotaxis. *P Natl Acad Sci USA*. 1999; 96:11346–11351.
31. Lutz R, Bujard H. Independent and tight regulation of transcriptional units in *Escherichia coli* via the LacR/O, the TetR/O and AraC/I1–I2 regulatory elements. *Nucleic Acids Res*. 1997; 25:1203–1210. [PubMed: 9092630]
32. Balch WE. Biochemistry of interorganelle transport. A new frontier in enzymology emerges from versatile in vitro model systems. *J Biol Chem*. 1989; 264:16965–16968. [PubMed: 2507534]
33. Guzman LM, Belin D, Carson MJ, Beckwith J. Tight regulation, modulation, and high-level expression by vectors containing the arabinose PBAD promoter. *J Bacteriol*. 1995; 177:4121–4130. [PubMed: 7608087]
34. Adler J. A method for measuring chemotaxis and use of the method to determine optimum conditions for chemotaxis by *Escherichia coli*. *J Gen Microbiol*. 1973; 74:77–91. [PubMed: 4632978]
35. Bainer R, Park H, Cluzel P. A high-throughput capillary assay for bacterial chemotaxis. *J Microbiol Methods*. 2003; 55:315–319. [PubMed: 14500024]

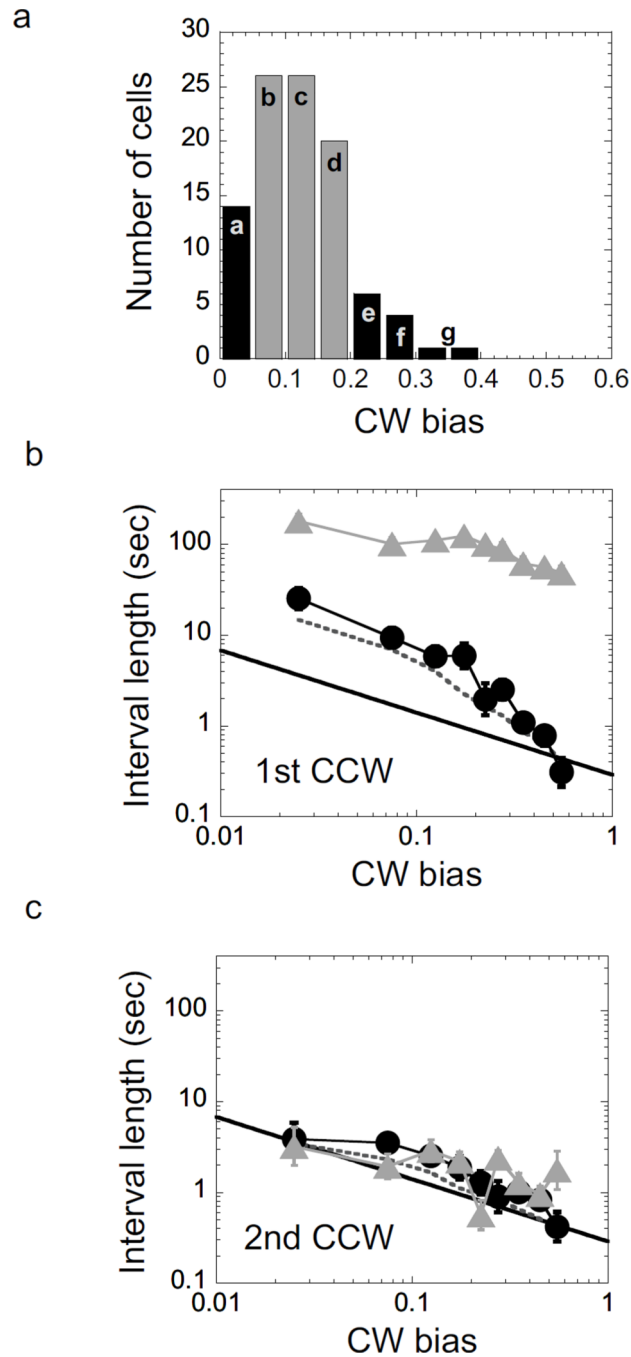


**Fig. 1. CCW interval lengths pre- and post-stimulus**

(A) Histogram of CW bias of wild-type cells. Grey bars are bins covering the average CW bias regime of wild-type cells. We sorted cells by their CW bias before stimulus and grouped them into the CW bias intervals (Methods). CW bias bins h and i are absent from the histogram because cells with CW bias greater than 0.4 require extra CheR from plasmid pZE21-CheR. We observed that most wild-type cells had CW biases between 0.05 and 0.2. To increase the chance to obtain cells with CW bias higher than 0.2, we transformed wild-type cells with pZE21-CheR (Methods). The first (B) and second (C) mean post-stimulus CCW interval lengths vs. pre-stimulus CW bias for all wild-type (RP437 and RP437 expressing CheR from pZE21-CheR) cells. (See Supplementary Fig. 1 for post-stimulus

CCW interval lengths in individual cells.) Black circles, cells exposed to a small stimulus (10 nM stepwise increase of L-aspartate). Grey triangles, cells exposed to a large stimulus (1  $\mu$ M stepwise increase of L-aspartate). Black line, power-law fit of the geometric mean of pre-stimulus CCW interval lengths calculated over 1500 s for all wild-type (RP437 and RP437 expressing extra CheR from pZE21-CheR) cells as a function of the pre-stimulus CW bias (Supplementary Fig. 1b). Error bars show the standard error associated with the average CCW interval length in each bin. Dark grey dotted line, geometric mean of the CCW interval lengths following a randomly chosen time point in non-stimulated cells. As the CW interval order after stimulus increases, the mean CCW interval lengths after stimulus approaches the mean CCW interval lengths (See also Supplementary Fig. 1).

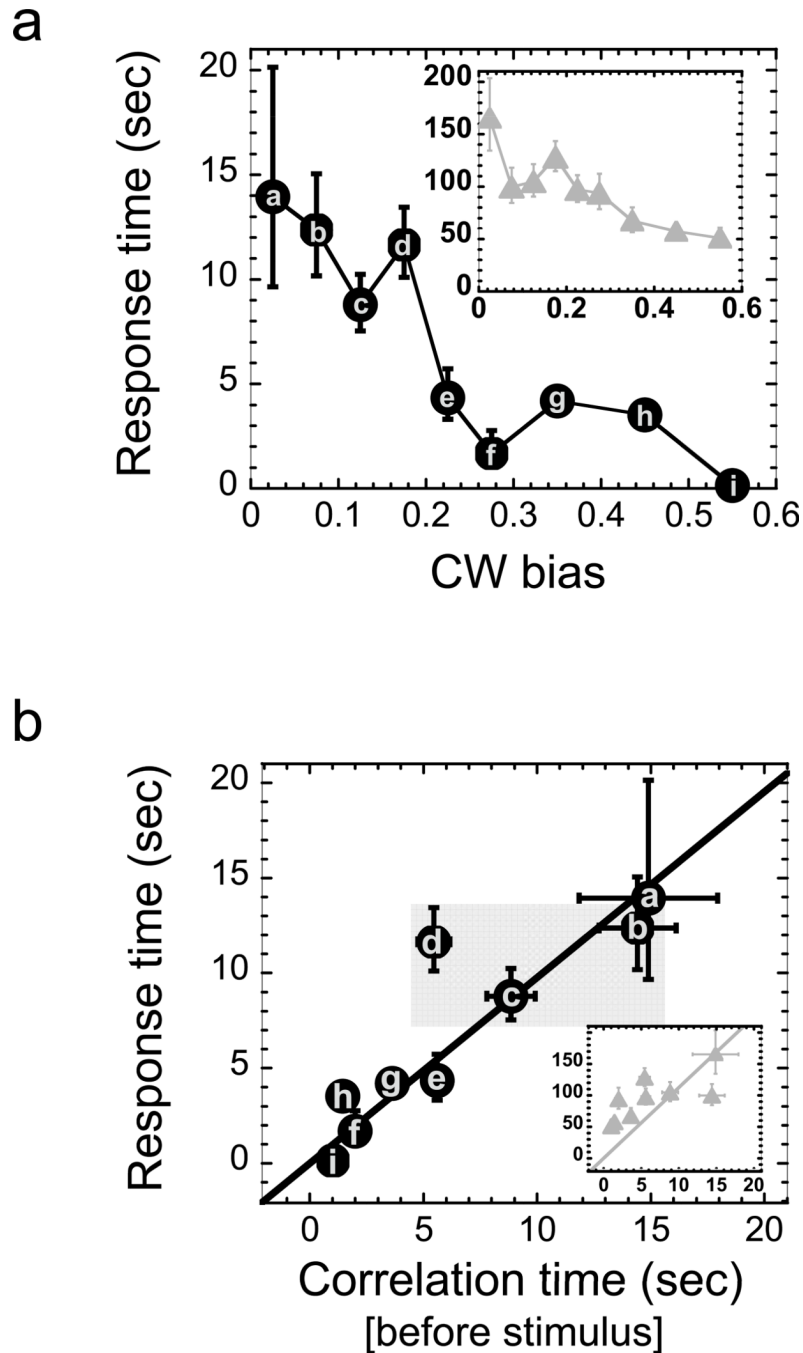


**Fig. 2. Response and adaptation to stepwise stimulus in cells with similar CW bias**  
**(A)** Average response time for wild-type (RP437 and RP437 expressing extra CheR from pZE21-CheR) cells exposed to a stepwise small (black circles, 10 nM L-aspartate) or large (**inset**; grey triangles, 1  $\mu$ M L-aspartate) stimulus. Error bars show the standard error associated with the average response time within each bin (a–i, Methods). **(B)** Average response time to a small (black circles) or large (**inset**, grey triangles) stimulus as a function of the correlation time for wild-type (RP437 and RP437 expressing CheR from pZE21-CheR) cells. For the large stimulus, the average response time was adjusted by a correction factor (Supplementary Fig. 2d). The solid lines are linear fit functions forced through the origin. Black line: Response time =  $C \cdot$  Correlation time.  $C \approx 0.98 \pm 0.10$  ( $R^2 = 0.75$ ). Inset grey

line: Relaxation time =  $C \cdot \text{Correlation time}$ .  $C \approx 12.23 \pm 1.83$  ( $R^2 = 0.07$ ). The letters correspond to CW bias bins (Methods). Error bars for the correlation time are the half lengths of the first uncorrelated CCW intervals. Error bars for the response time are the standard error associated with the average response time within each bin. Grey area, peaks of wild-type cell population.

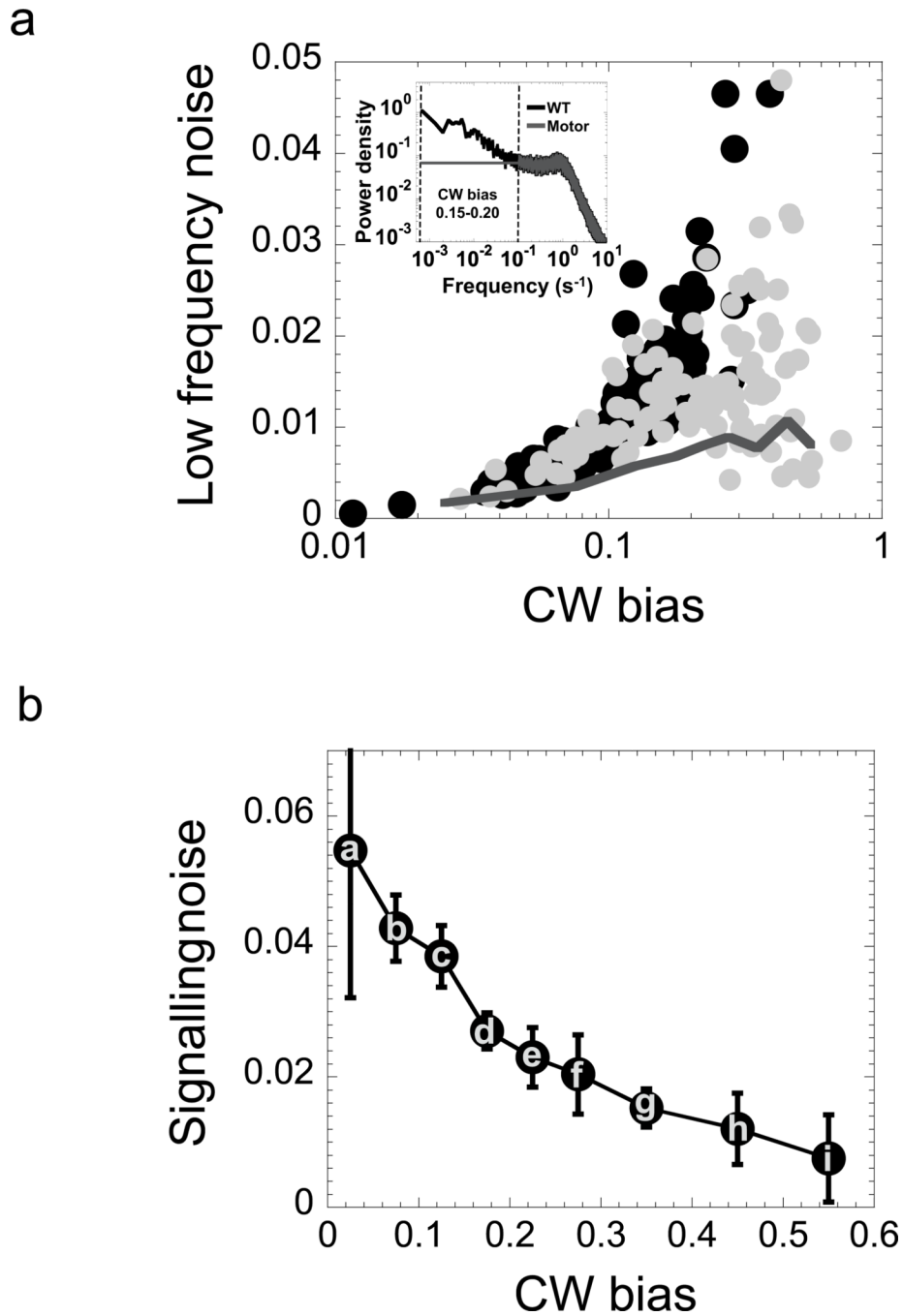


**Fig. 3. Low frequency noise in non-stimulated cells**

(A) Low frequency noise in individual wild-type RP437 cells (black) and RP437 cells expressing CheR from pZE21-CheR (grey) versus CW bias. (**Inset**) Power spectral density (black) averaged over wild-type cells (RP437 and RP437 cells expressing CheR from pZE21-CheR) with CW bias = 0.15–0.20 (see Supplementary Fig. 5 for all CW bias bins). Power spectral density (dark grey line) of the motor decoupled from the signalling network<sup>3</sup> (See Supplementary Fig. 5 for all CW bias bins). We determined the low frequency noise for the region between the dotted lines.

**(B)** Signalling noise as a function of CW bias for wild-type RP437 cells and RP437 cells expressing CheR from pZE21-CheR. Signalling noise is defined as the variance ( $\sigma_{CheYp}^2$ ) of the fluctuating [CheY-P]. Letters correspond to the CW bias bins (Methods). The power spectral densities and CW biases are averaged over cells within the same CW bias. Error bars show the standard error associated with the estimated signalling noise within each bin.

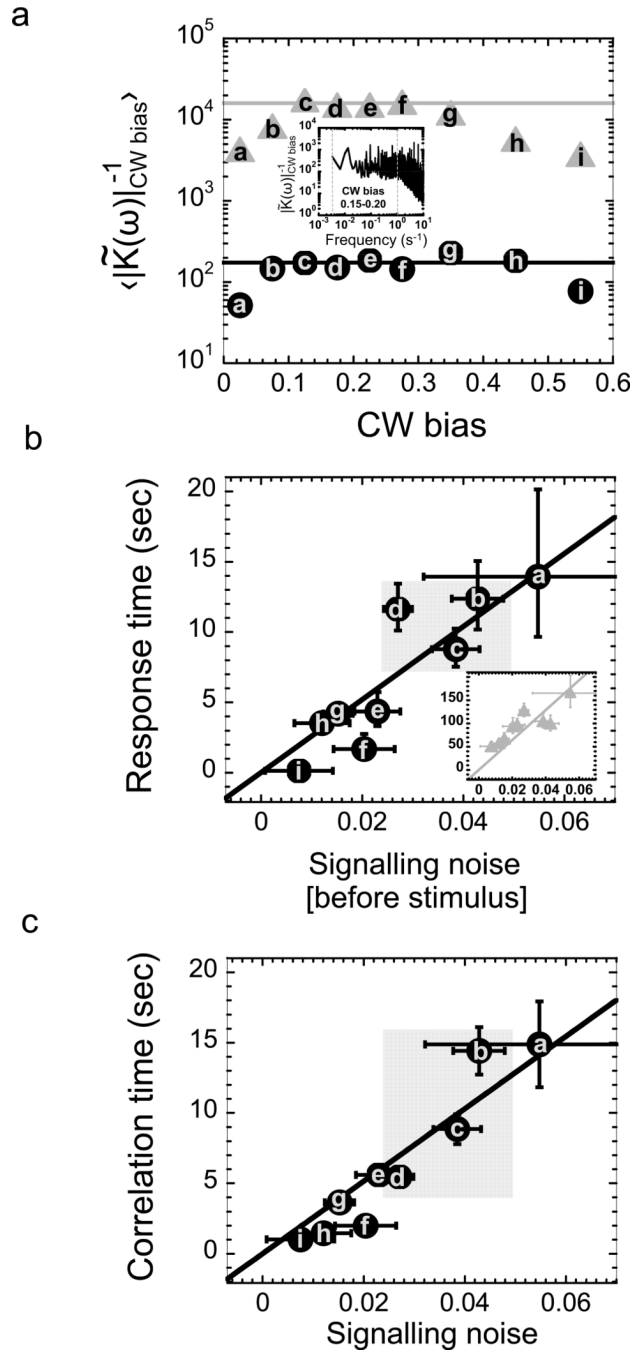


**Fig. 4. Relationship between signalling noise and cellular response to a small external stimulus**

(A) Inverse of the coupling coefficient  $|\tilde{K}(\omega)|_{CW\ bias}^{-1} = \frac{1}{\omega} \frac{|\tilde{\mu}(\omega)|}{|\tilde{C}(\omega)|}$  averaged over the long timescale for which this ratio is constant for the small (black circles) or large (grey triangles) stimulus. We computed the geometric mean over frequencies ranging from 1 s to 5 min for a small stimulus (from 10 s to 5 min for a large stimulus) in each CW bias bin. Standard error of the mean is smaller than the marker size. Lines, mean value of  $|\tilde{K}(\omega)|_{CW\ bias}$  computed over CW biases ranging from  $\sim 0.05$  to 0.5 for a small stimulus (black) and from  $\sim 0.1$  to 0.3 for a large stimulus (grey). (Inset) Inverse of  $|\tilde{K}(\omega)|_{CW\ bias}$  for CW bias ranging from 0.15 to

0.20 for a small stimulus (10 nM L-aspartate increase) released at  $t = 0$ . See Supplementary Fig. 7 for all CW bias bins. **(B)** Average response times of wild-type (RP437 and RP437 expressing inducible CheR) cells to small (black circles) or large (**inset**, grey triangles) stimulus versus mean pre-stimulus signalling noise. Solid lines, linear fits forced through the origin: Response time =  $C \times \sigma_{CheYp}^2$ . Black line:  $C = 259 \pm 25 \text{ sec}/\mu\text{M}^2$  ( $R^2 = 0.8$ ) for small stimulus. **Inset**, grey line:  $C = 3215 \pm 307 \text{ sec}/\mu\text{M}^2$  ( $R^2 = 0.4$ ) for large stimulus. Grey area, average functioning state of wild-type population. **(C)** The correlation time as a function of the mean signalling noise before stimulus for wild-type (RP437 and RP437 expressing CheR from pZE21-CheR) cells. Black line, linear fit function forced through the origin (Correlation time =  $C \times \sigma_{CheYp}^2$ ;  $C \approx 257 \pm 21 \text{ sec}/\mu\text{M}^2$  ( $R^2 = 0.9$ )). Error bars for the correlation time are the average half-lengths of the first uncorrelated CCW intervals. Error bars for the signalling noise are the standard error associated with the signalling noise in each bin. Grey area is the average functioning state of wild-type population. Letters correspond to the CW bias bins (Methods).